RSC Advances

PAPER

Cite this: *RSC Adv.*, 2022, **12**, 31142

Simultaneous CO_2 reduction and NADH regeneration using formate and glycerol dehydrogenase enzymes co-immobilized on modified natural zeolite†

Clarissa Cocuzza,[a] Giuseppe Pietricola,[a] Ilaria Zonca,[a] Melodj Dosa,[a] Oscar Romero,[c] Tonia Tommasi,[a] Valentina Cauda,[a] Debora Fino,[a] Carminna Ottone *[b] and Marco Piumetti *[a]

In this work, the co-immobilization of formate dehydrogenase (FDH) and glycerol dehydrogenase (GlyDH) enzymes is proposed to reduce CO_2 into formic acid, an important chemical intermediate. The reduction of carbon dioxide is carried out by FDH to obtain formic acid, simultaneously, the GlyDH regenerated the nicotinamide cofactor in the reduced form (NADH) by the oxidation of glycerol into dihydroxyacetone. Natural zeolite was selected as immobilization support given its good properties and low cost. The natural zeolite was modified with subsequent acid-alkaline attacks to obtain a mesostructurization of the clinoptilolite. The two enzymes were co-immobilized on clinoptilolite, previously hetero-functionalized with amino and glyoxyl groups. The distribution of the enzymes was confirmed by fluorescence microscopy analysis. Furthermore, a great increase in the retained activity for the formate dehydrogenase enzyme was noted, passing from 18% to 89%, when the mesostructured clinoptilolite was used as support. The immobilization yield of formate dehydrogenase and glycerol dehydrogenase is around 100% with all the supports studied. The promising results suggest a possible development of this procedure in enzyme immobilization and biocatalysis. The biocatalysts were characterized to find the optimal pH and temperature. Furthermore, a thermal stability test at 50 °C was carried out on both enzymes, in free and immobilized forms. Finally, it was shown that the biocatalyst is effective in reducing CO_2, both by using the cofactor in the reduced form (NADH) or the oxidized form (NAD^+), obtaining NADH through the regeneration with glycerol in this latter case.

Received 3rd June 2022
Accepted 24th October 2022

DOI: 10.1039/d2ra03459j

rsc.li/rsc-advances

1 Introduction

In the last two centuries, research in catalysis was focused on pursuing greener and more sustainable technologies for the abatement of atmospheric contaminants and the formation of high-value-added molecules from waste.[1,2] Carbon dioxide (CO_2) is the predominant greenhouse gas generated both from anthropogenic and natural sources, and its emissions are realistically impossible to nullify. On the other hand, CO_2 is involved in several industrial processes, and it could be considered a reagent to produce organic compounds such as urea and salicylic acid.[3] As a result, the catalytic reduction of CO_2 into high-value-added products or chemical intermediates to decrease its high concentration in the atmosphere has been proposed in recent studies.[1,4]

Mimicking the natural photosynthetic mechanism is a viable route, it is considered an alternative to the more energy-consuming classical heterogeneous catalysis, alongside exploiting biological systems, namely microbial metabolic pathways and enzyme-mediated processes.[3,4] Using cellular systems such as bacteria or fungi lead to cheaper processes, decreasing both the operative and the downstream costs. However, they require more stringent operative conditions regarding temperature, pH, aeration, and nutrient supply.[2] On the other hand, the production of enzymes is generally more expensive, but since they are single proteins catalyzing single reactions, they provide an incomparable selectivity to the desired product, making the purification process easier and cheaper. Over the years, various enzymes, mainly in the classes of oxidoreductases and lyases, have been investigated to yield

[a]*Department of Applied Science and Technology, Politecnico di Torino, Corso Duca degli Abruzzi 24, I-10129 Turin, Italy. E-mail: marco.piumetti@polito.it; Tel: +39 011 0904753*

[b]*Escuela de Ingeniería Bioquímica, Pontificia Universidad Católica de Valparaíso, Av. Brasil 2085, Valparaíso, Chile. E-mail: carminna.ottone@pucv.cl; Tel: +56 32 2372018*

[c]*Bioprocess Engineering and Applied Biocatalysis Group, Departament of Chemical, Biological and Enviromental Engineering, Universitat Autònoma de Barcelona, 08193, Spain*

† Electronic supplementary information (ESI) available. See DOI: https://doi.org/10.1039/d2ra03459j

carbon-based chemicals with higher value, including methane, methanol, and carbohydrates.[5]

Obert and Kuwabata developed the first enzymatic cascade reactions to reduce CO_2 into methanol.[6,7] The process proposed by Obert seems to be very promising and entails three dehydrogenases to work as an assembly line, with the consumption of three moles of reduced nicotinamide adenine dinucleotide cofactor (NADH) for a mole of methanol produced.[6] The mechanism mainly consists of the reverse oxidation of methanol: the first enzyme, formate dehydrogenase (FDH, EC 1.2.1.2), carries out the reduction of carbon dioxide into formic acid; then a second oxidoreductase, formaldehyde dehydrogenase (FaldDH, EC 1.2.1.46), converts formate into the corresponding aldehyde; eventually, alcohol dehydrogenase (ADH, EC 1.1.1.1) reduces formaldehyde into methanol.[3,6] To obtain better performance, previous studies in the literature suggest using carbonic anhydrase to increase the CO_2 solubilization in the reaction medium, before performing the cascade reactions previously described.[8] The first step of this cascade reaction is studied in this paper, using the enzyme FDH co-immobilized with glycerol dehydrogenase (GlyDH, EC 1.1.1.6). The second enzyme is necessary to perform a cofactor regeneration during the CO_2 reduction reaction.

In fact, in addition to the problems derived from the expensive and burdensome production of the enzymes, and the stable maintenance of their three-dimensional structure, the high cost of the cofactor is another critical issue to scale up this process to the industrial level.[5,9] As far as the regeneration of cofactor NADH is concerned, it requires the delivery of electrons to the oxidized form of the molecule. Different approaches have been designed and studied, such as electrochemical, photochemical, and biochemical processes.[10–12] The exploitation of solar energy or electricity from renewable sources may be a promising solution for greener applications. However, by using enzymes good efficiency and selectivity have been obtained. Furthermore, it is not necessary to use expensive mediators, such as molecules based on noble metals.[5] By using the glycerol dehydrogenase enzyme, it is possible to regenerate the NADH cofactor[13] and at the same time, the organic waste from the biodiesel industry can be valorized. This enzyme performs the oxidation of glycerol to dihydroxyacetone using one mole of the oxidized cofactor, returning the reduced form NADH. This reaction has several advantages: the oxidized form of the cofactor (NAD^+) is regenerated to NADH and dihydroxyacetone (DHA) is obtained as a co-product, DHA has a market value of about twenty-five times the value of glycerol.[14] Finally, there is the possibility to valorize a by-product of the biodiesel industry, which can potentially be almost cost-free.

Furthermore, the immobilization of enzymes will allow the re-using of them, lowering their cost of application. The immobilization process is a critical point because the environment in which the reactions occur significantly affects the global performance of the enzyme: the confinement into materials with specific morphologies and the co-presence of other enzymes in the surroundings are two conditions that can modify the behavior of the enzyme.[15] Among all the possible materials, inorganic porous supports, such as silica and zeolites, present good features and are very suitable for enzyme immobilization, although in some cases it is necessary to change the zeolites' morphology due to their reduced pore size.[15–17] Natural zeolites such as clinoptilolite can be used as a valid alternative to synthetic ones due to their low cost. Furthermore, they have the advantage of being materials that are widespread in different parts of the world.[18,19] Their porous structure can be improved to satisfy the working parameters of a specific process, for example, through a mesostructuring procedure.[20] In this way, it is possible to minimize the mass transfer phenomena, caused by too small porosities, and increase enzymatic stability. In particular, zeolites are well-suited for the covalent immobilization technique, which ensures the proper holding of the protein, minimizing the risk of leakage.[21] Zeolites can be hetero-functionalized, with glyoxyl and amino groups, to perform a two-step covalent immobilization strategy: the first step at neutral pH enhances the immobilization yield by ionic interactions without damaging the activity of the enzyme; the second step at basic pH allows the multipoint covalent interactions.[22] Since the immobilization of enzymes over solid supports involves strong bonds between the support and specific amino acids, this strategy has to be carefully optimized to avoid changes in the conformation of the active site of the protein.[23] The multipoint covalent strategy, despite increasing the rigidity of the immobilized enzymes, makes them more stable in the presence of distorting reagents.[24,25]

In this work, the Candida boidinii FDH enzyme is used along with the geobacillus stearothermophilus GlyDH enzyme to investigate the reduction of CO_2 to formic acid, the first step of the cascade reactions proposed by Obert and Kuwabata.[6,7] For the first time to our knowledge, both the GlyDH and FDH enzymes were co-immobilized covalently on natural zeolite to perform the CO_2 reduction and simultaneously the regeneration of the NADH cofactor. The clinoptilolite was modified with subsequent acid and alkaline attacks to alter its morphology making it more suitable for enzyme immobilization.[26] Two different processes of mesostructuring were tested. The first one involved an ion exchange of the original cations of the framework before the mesostructuring process. Instead, the second used the natural zeolite with the native cations originally occupying the cavities of the framework. Subsequently, the zeolites were hetero-functionalized, and finally, FDH and GlyDH were co-immobilized on the support.

The co-immobilization of the two enzymes on the support decreases the delay of the regeneration of the cofactor in its reduced form (NADH) compared to a similar process with FDH and GlyDH immobilized on separate particles, increasing the efficiency of the CO_2 reduction. With FDH and GlyDH separately supported, the cofactor would be diluted in a medium and would need more time to migrate from one enzyme to the other. On the other hand, the co-immobilization strategy also has some drawbacks, for example, ones related to the different stability conditions of distinct enzymes. This is another reason why it is important to find operative parameters suitable for both enzymes.[27] Another important aspect is the distribution of the FDH and GlyDH on the surface of the support; this can be

investigated with fluorescence microscopy. The biocatalyst (enzyme immobilized on support) was also characterized through the retained activity (R_{act}) and immobilization yield (IY). In addition, the optimum pH and temperature were evaluated as well as the stability factor obtained after the immobilization. Finally, the biocatalyst was tested to carry out the CO_2 reduction reaction through FDH. The CO_2 reduction was performed using the oxidized form of the nicotinamide cofactor (NAD^+) and GlyDH enzyme to regenerate the cofactor, thus confirming the regeneration process of NADH.

2 Materials and methods

2.1 Materials

(3-Glycidyloxypropyl)trimethoxysilane (GPTMS, ≥98%), (3-aminopropyl)triethoxysilane (APTES, ≥98%), sulfuric acid (≥98%), sodium borohydride (≥98%), sodium hydroxide (97%), toluene (99.8%) and hydrochloric acid (37%) were supplied from Sigma-Aldrich. Sodium formate, sodium metaperiodate, and glycerol (86%) were purchased from Merck. Formate dehydrogenase (FDH) from *Candida boidinii* with a protein concentration of 25 ± 1 mg mL^{-1} (according to Bradford assay[28]) was purchased from Megazyme. NAD^+ (99.6%) was supplied from PanReach AppliChem. Base Clinoptilolite (B-Clino) was supplied by Zeolado (Greece). Glycerol dehydrogenase (GlyDH) from *Geobacillus stearothermophilus* was produced and purified as previously reported.[29]

2.2 Methods

2.2.1 Preparation of mesostructured zeolites. The two samples of mesostructured clinoptilolite (M-Clino and M-Na-Clino) were prepared by adapting the method reported by Moradi *et al.*[30] Clinoptilolite with a Si/Al ratio in the range of 4.0 to 5.3 was first washed with ultrapure water (Milli-Q) at room temperature for 10 minutes. Next, a dealumination process was performed with HCl 1 M at 100 °C for 4 h. This treatment was repeated 4 times to remove the aluminum in excess, which is reported to be detrimental to the mesostructuring process. After the dealumination process, an alkaline desilication was carried out with NaOH 0.2 M at 100 °C for 30 minutes, followed by a milder acid wash with HCl 0.5 M at the same temperature for 4 h, to remove the aluminum on the surface. After each dealumination and desilication treatment, the zeolites were centrifugated, washed, and dried overnight at 60 °C. The sample of mesostructured sodium-clinoptilolite (M-Na-Clino) was obtained by replacing the washing with Milli-Q water with an ion exchange with NaCl 2 M at 50 °C for 3 h, to have sodium ions on the framework of the clinoptilolite instead of the native cations of the framework. The other steps are the same described above.

2.2.2 Supports functionalization. All the zeolites (B-Clino, M-Clino, and M-Na-Clino) were hetero-functionalized with glyoxyl and amino groups, using respectively GPTMS and APTES, by adapting the method reported in the literature from Bernal *et al.*,[31] Pietricola *et al.*[16] and Cesar *et al.*[8] The formation of glyoxyl groups went through a series of three reactions: firstly, the generation of epoxy groups on the surface of the support, then the hydrolysis with sulphuric acid, with the opening of the ring structure to form diols, and finally the oxidation of the latter with sodium periodate to yield glyoxyl groups. For each sample, 1 g of zeolite was put into a balloon with GPTMS and APTES, both 5% v/v, in 30 mL of toluene at 105 °C for 5 h. To avoid the evaporation of the solvent, the glass round-bottom flask was connected to a water-cooling column. Then, the solid was filtered and thoroughly washed with acetone and water. Hydrolysis of epoxy groups was carried out by putting the powder in contact with 30 mL of sulphuric acid in a concentration of 0.1 M at 85 °C for 2 h. Again, it followed a step of filtration and deep washing with abundant distilled water. The last stage of functionalization was the oxidation of diol groups by 30 mL of sodium periodate aqueous solution 0.1 M at room temperature for 2 h more, followed by one last filtration and washing with distilled water and phosphate buffer 25 mM pH 7 to remove periodate ions from the surface. The quantification of glyoxyl groups on the surface of the materials was performed by a back-titration method, as reported by Guisan.[32] The moles were calculated by exploiting eqn (1)

$$\frac{\mathrm{mol_{gly}}}{m_{\mathrm{sup}}} = \frac{1}{m_{\mathrm{sup}}} V_{IO_4^-} \left[IO_4^-\right]_{\mathrm{in}} \left(1 - \frac{\mathrm{Abs_{final}}}{\mathrm{Abs_{init}}}\right) \times 1000 \qquad (1)$$

where the amount of glyoxyl groups are expressed in μmol, m_{sup} the mass of support subjected to functionalization (g), $V_{IO_4^-}$ is the volume of the $NaIO_4$ solution (mL), $[IO_4^-]$ is the concentration of IO_4^- ions in the latter (mmol mL^{-1}), and Abs_{init} and Abs_{final} are the values of absorbance measured, for the supernatant at the beginning and at the end of the oxidation, at 420 nm. The functionalization resulted to be efficient for all supports. All zeolites have a functionalization yield of around 300 μmol g^{-1} (in detail: B-Clino 273 μmol g^{-1}; M-Clino 332 μmol g^{-1}; M-Na-Clino 304 μmol g^{-1}).

2.2.3 Activity assay. 50 μL of FDH solution (0.05 mg mL^{-1} according to Bradford assay[28]) or 5 mg of support (with FDH immobilized) was added to a solution of 2.3 mL of 0.1 M phosphate buffer pH 7.5, 100 μL of cofactor NAD^+ 50 mM and 500 μL of sodium formate 0.3 M. Similarly, 100 μL of GlyDH solution (0.05 mg mL^{-1} according to Bradford assay[28]) or 5 mg of support (with GlyDH immobilized) was added to 1.850 mL of glycerol solution 100 mM (in 0.1 M phosphate buffer pH 7) and 50 μL of NAD^+ 100 mM. The increase in absorbance at 340 nm, corresponding to the peak of formation of NADH, was recorded for two minutes and correlated to the specific activity of the free enzyme (A_{FE}, in UI mg_{prot}^{-1}) and immobilized (A_{IE}, in UI g_{sup}^{-1}). The activity is expressed in IU (international unit) and corresponds to the amount of enzyme necessary to produce one μmol per minute of NADH at the defined conditions of pH and temperature.

2.2.4 Immobilization and co-immobilization of FDH and GlyDH on supports. The immobilization was carried out in two different ways. In the first case, the two enzymes were immobilized separately, while in the second case a co-immobilization was carried out by immobilizing the two enzymes at the same time. In this way, 1 g of support was put in contact with 2 mg of FDH or 2 mg of GlyDH. The process was adapted from Pietricola *et al.*[16] and Rocha-Martin *et al.*[29] First, FDH or GlyDH was

dissolved in 20 mL of 25 mM phosphate buffer pH 7, and this mixture was maintained at a temperature of 4 °C in an ice bath, with gentle stirring. After adding the support, the immobilization took place, and the time of immobilization was estimated by collecting samples of the supernatant and monitoring the activity of the enzyme still in solution. At the same time, enzyme activity under the same conditions, but not in contact with the support, was evaluated and used as a blank. When the activity of the supernatant in the immobilization solution dropped to zero or remained constant for two consecutive measurements, the mixture was filtered under vacuum in a Buchner funnel. Subsequently, the solid was resuspended in 20 mL of 100 mM carbonate buffer pH 10 for 30 minutes. Afterward, 10 mg of sodium borohydride was added to the mixture with 5 mL of glycerol, to reduce the Schiff's bases formed between the glyoxyl groups of the functionalized support and the amino groups of the enzyme. After 10 minutes, the solid was filtered under vacuum, washed with abundant water and 25 mM phosphate buffer pH 7, and dried in a desiccator at the temperature of 4 °C. Next, Bradford assay[28] was carried out to determine the concentration of protein at the beginning (C_{prot,t_0}) and at the end (C_{prot,t_f}) of the immobilization process. Finally, the immobilization yield (IY) was evaluated and expressed in eqn (2) as:

$$\mathrm{IY}\ (\%) = \frac{C_{\mathrm{prot},t_0} - C_{\mathrm{prot},t_f}}{C_{\mathrm{prot},t_0}} \times 100 \quad (2)$$

The activity of the immobilized enzyme can be expressed in the form of the retained activity (R_{act}) shown in eqn (3) as:

$$R_{\mathrm{act}}\ (\%) = \frac{A_{\mathrm{IE}}}{q \times A_{\mathrm{FE},t_0}} \times 100 = \frac{A_{\mathrm{IE}}}{C_{\mathrm{act}}} \times 100 \quad (3)$$

where A_{IE} is the specific activity of the immobilized enzyme (in UI g_{sup}^{-1}), q is the enzymatic load provided in $mg_{\mathrm{prot}}/g_{\mathrm{sup}}$, A_{FE,t_0} is the specific activity of the free enzyme at the beginning of the immobilization (in UI mg_{prot}^{-1}), calculated as described in Section 2.2.5. C_{act} represents the contact activity, namely the maximum specific activity of the support if all the protein in contact was immobilized and fully active.

2.2.5 Characterization of materials. The specific surface area (S_{BET}) of the samples of zeolite involved in this work was evaluated by nitrogen physisorption at −196 °C, with a Micromeritics TriStar II 3020 instrument and then by processing the results with the Braunauer–Emmet–Teller method (BET). However, for zeolites, the BET method usually provides quite underestimated values of the surface area, hence it was also calculated with the Langmuir method S_{LAN}. Furthermore, the micropores volume (V_{micro}) were evaluated by analyzing the desorption stage with the Barrett–Joyner–Halenda (BJH) method. Before testing, all the samples were subjected to an outgassing pre-treatment at a high temperature (400 °C) for 2 h to remove impurities on the surface of the support. The crystalline structure of materials was determined with X-ray diffractometry (XRD) by using an X'Pert Philips PW3040 diffractometer using Cu Kα radiation (2θ range = 5°–40°; step = 0.05° 2θ; time per step = 0.2 s). The diffraction peaks were compared according to the Powder Data Files database (PDF 2000). Sample morphology was analyzed through FE-SEM microscopy (Zeiss MERLIN, Gemini-II column) and HR-TEM microscopy (JEM-3100F, FE-LaB_6 gun). Infrared measurements were carried out on the three functionalized supports B-Clino, M-Clino, and M-Na-Clino. IR spectra were acquired on Bruker INVENIO equipped with liquid nitrogen cooled MCT detector. The Fourier transform IR (FT-IR) spectra were collected, after a pretreatment of 1 hour at 300 °C in standard vacuum conditions, at room temperature, and atmospheric pressure in the range of 4000–400 cm^{-1} with 64 scans and a resolution of 4 cm^{-1}. The analyses were performed on pellets, obtained by pressing the sample powder at 150 bar, and the intensity was normalized by dividing it by the surface density of the pellet.

2.2.6 Temperature and pH profile of biocatalyst. The temperature and pH profiles of the biocatalysts were evaluated by calculating the activity, as expressed in Section 2.2.5, varying only the pH or temperature. Specifically, to evaluate the pH profile, the temperature was kept fixed at 30 °C and the pH of the solution varied from 6 to 10. A 0.1 M phosphate buffer was used for pH 6, 7, and 8 solutions while a 0.1 M carbonate buffer was used for pH 9 and 10 solutions. To evaluate the temperature profile, activity tests at a temperature ranging from 30 to 60 °C were carried out (at pH 7.5 for FDH enzyme and 7 for GlyDH enzyme).

2.2.7 Thermal stability of free and immobilized enzymes. Both free and immobilized enzymes were incubated at 50 °C. To evaluate the residual activity over time, an activity test was carried out as described previously, at 30 °C (at pH 7.5 for FDH enzyme and 7 for GlyDH enzyme). The residual activity (A) was expressed as a percentage of the initial activity (A_0). To describe the deactivation of the free enzyme, a first-order deactivation model with no residual activity was used, expressed in eqn (4) as:

$$A = A_0 \times \mathrm{e}^{-k_{\mathrm{D}}t} \quad (4)$$

where k_{D} represents the deactivation constant (h^{-1}) and t is the time (h). Conversely, immobilized enzymes were more likely to follow an asymptotic deactivation model, which can be described by eqn (5):

$$A = A_0[(1 - \alpha)\mathrm{e}^{-k_{\mathrm{D}}t} + \alpha] \quad (5)$$

where α is the residual activity at infinite time. From eqn (4) and (5) it was possible to obtain the half-life ($t_{1/2}$) and finally the stabilization factor (S_{F}), expressed in eqn (6):

$$S_{\mathrm{F}} = \frac{t_{1/2,\mathrm{imm.\ enz.}}}{t_{1/2,\ \mathrm{sol.\ enz.}}} \quad (6)$$

2.2.8 Co-immobilization of fluorescence-labeled enzymes. FDH and GlyDH were labeled with ATTO 488 and ATTO 550, respectively, using a protein labeling kit and separation columns (from Sigma Aldrich) according to the procedure indicated by the manufacturer, a similar procedure is also reported in the literature by Rocha-Martín *et al.*[33] Each enzyme was incubated in soluble form with the respective dye for 2 h at

pH 9.5 (carbonate buffer 0.1 M) and purified into a separation column. Immobilization and co-immobilization of the labeled enzymes were carried out in the dark, following a similar procedure to the non-labeled enzymes, previously described. B-Clino was chosen as a support because it did not show any fluorescence emittance in the considered wavelength range, unlike the mesostructured supports. The sample was deposited on a glass slide and covered with a cover-glass slip, then observed with a Nikon Eclipse Ti-e fluorescence optical inverted microscope, at 100× magnification. The microscope is equipped with a super bright wide-spectrum source (Shutter Lambda XL), a high-resolution camera (Zyla 4.2 Plus, 4098 × 3264 pixels, Andor Technology) and an immersion oil 100× objective (Nikon). Fluorescence filters were set to an excitation centered at 488 nm (obtaining a green light emission) and an excitation centered at 550 nm (obtaining a red light emission). The collected images were analyzed with the NIS-Element software (NIS-Element AR 4.5, Nikon). A merge of brightfield, green and red emission images was performed to obtain co-localization images where the two fluorescence signals collected result to be superimposed.

2.2.9 Reduction of CO_2 into formic acid. The reduction of CO_2 to formic acid was conducted in a sealed glass bottle, at 30 °C under stirring, 1 atm, and pH between 6.5 and 7.5, blowing CO_2 in solution during all the tests. For each reaction, 500 mg of biocatalyst were suspended into 30 mL of phosphate buffer 100 mM pH 7.5 and, to ensure a solution constantly saturated with carbon dioxide, 100 mL min^{-1} of CO_2 was bubbled from the bottom, causing the pH to decrease. Firstly, only FDH was supported over M-Clino, and 10 mM of NADH was dissolved into the initial solution, to assess the single reaction. Secondly, FDH and GlyDH were co-immobilized over M-Clino, and the initial feed was 10 mM of NAD^+ and equimolar glycerol. In this way, the chain reaction of conversion of cofactor and reduction of CO_2 was studied. The variation of formic acid concentration was observed in a Shimadzu 20A prominence device, equipped with an RDA detector at 210 nm, on a Kinetex Phenomenex C18 (4.6 × 250 mm, 10 μm) column kept at 30 °C. The mobile phase used was 5 mM sulphuric acid in Milli-Q water, the flow rate was 0.4 mL min^{-1}, and the retention time is 3.1 minutes.

3 Results and discussion

3.1 Support characterization

3.1.1 Nitrogen physisorption at 77 K. To create a mesoporous structure inside the clinoptilolite that is more suitable for enzyme immobilization, the natural clinoptilolite was subjected to two different treatments. The structure of the resulting three materials, untreated clinoptilolite (B-Clino), mesoporous clinoptilolite (M-Clino), and ion exchange mesostructured clinoptilolite (M-Na-Clino) were characterized.

Table 1 summarizes the results obtained from nitrogen physisorption tests (BET surface area S_{BET}, Langmuir surface area S_{Lang}, pore volume V_p, and micropore volume V_{micro}). The specific surface area of clinoptilolite (B-Clino) is relatively low, this can be ascribed to the fact that it is a natural zeolite. Due to the mesostructuring process, the S_{BET} of clinoptilolite increased by 427% for M-Clino and 454% for M-Na-Clino while S_{Lang} increased by 662% for M-Clino and 697% for M-Na-Clino. This outcome is also observable from the change of shape and position of the isotherms (Fig. 1). The pore size distribution of both mesostructured samples showed multi-modal behavior, with peaks in the meso-macroscopic range between 30 and 200 nm (Fig. S1†). Isotherms of the nitrogen physisorption test, alongside pore size distribution diagrams, were reported to show the entity of Slit-like porosity, typically generated by the flaky morphology of clinoptilolite particles, which was further confirmed by the shape of the hysteresis. Furthermore, the values of the volume of micropores of M-Clino and M-Na-Clino were increased due to acid/alkaline attacks, (total pore volume of the modified clinoptilolites was increased too but to a lesser extent compared to V_{micro} values).

Table 1 Results of nitrogen physisorption tests and mesostructuring process

	B-Clino	M-Clino	M-Na-Clino
S_{BET} ($m^2\ g^{-1}$)[a]	37	195	216
S_{Lang} ($m^2\ g^{-1}$)[b]	39	282	311
V_p ($cm^3\ g^{-1}$)[c]	0.14	0.22	0.25
V_{micro} ($cm^3\ g^{-1}$)[d]	0.005	0.064	0.066

[a] Specific surface area obtained through the BET method. [b] Specific surface area obtained through the Langmuir method. [c] Total pore volume, calculated with the BJH method. [d] Volume of micropores calculated applying the *t*-plot method.

The mesostructuring process (Fig. S1†). In addition, in our previous work, it was reported that the functionalization procedures with APTES and GPTMS do not affect the mesoporosity of material.[16]

3.1.2 XRD. The XRD patterns of the studied samples are reported in Fig. 2. The clinoptilolite diffractogram (B-Clino) exhibits a high crystallinity pattern with its well-known peaks at 2θ = 9.75, 22.34, and 29.98° which are indexed with the

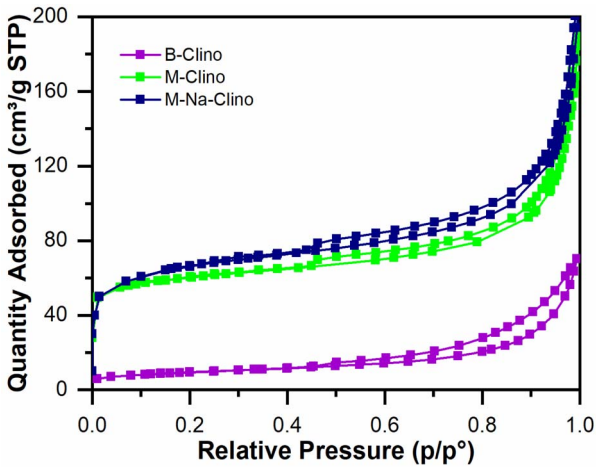

Fig. 1 Isotherms from nitrogen physisorption tests for the base (B-Clino) and the mesostructured (M-Clino, M-Na-Clino) clinoptilolite samples.

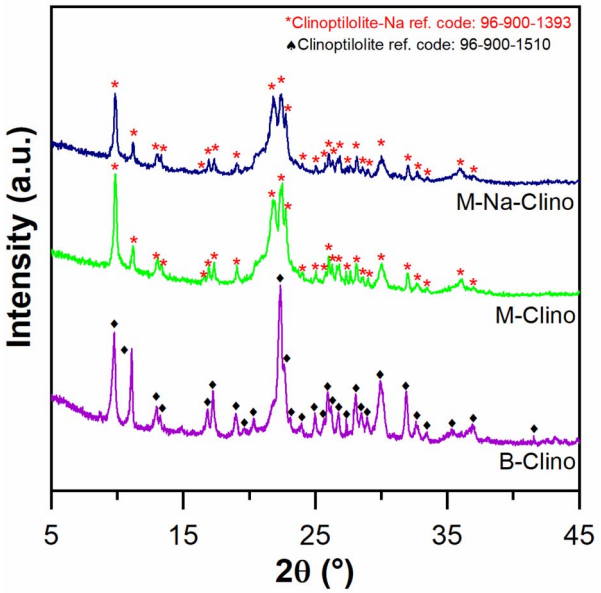

Fig. 2 XRD diagram comparison between B-Clino, M-Clino, and M-Na-Clino.

clinoptilolite reference code: 00-039-1383. Furthermore, the modified M-Clino and M-Na-Clino preserve the same characteristics peaks of B-Clino. However, it is possible to observe a decrease in the peak intensities in these two materials. The reason could be due to the acid/alkaline treatment used for the mesostructuring process which allows new cavities and pores, but irreversibly changes the B-Clino crystal structure. It is possible to observe a new additional peak at about 22°. This new peak can be ascribed to the presence of Na in the structure of M- and M-Na-Clino. The reference pdf number is ascribed to Na-clinoptilolite (reference nr. 96-900-1393). The presence of Na in M-Na-Clino is clearly explained due to the ion-exchange treatment to obtain this element inside the clinoptilolite structure. On the other hand, for M-Clino the presence of Na could be explained by the desilication treatment with NaOH. When the B-Clino reacts in NaOH solution, the desilication process occurs because the Si inside clinoptilolite was exchanged with Na^+ from NaOH. Thus, in M-Clino, there is a small amount of Na.

3.1.3 Electron microscopy. With electron microscopy analysis, the morphology of the support at different levels of magnification was defined. Fig. 3 compares FE-SEM images of B-Clino (a, b) M-Clino (c, d), and M-Na-Clino (e, f) at 1k× and 10k× magnification. Likewise, Fig. 4 displays B-Clino, M-Clino, and M-Na-Clino subjected to HR-TEM analysis at different magnifications. As previously mentioned, Fig. 3 demonstrates the flaky morphology of clinoptilolite, which was substantially maintained during the acid/alkaline attacks. From a macroscopic point of view, the particles of M-Clino appear to be slightly larger, as if some sort of aggregation took place (Fig. 3c). On the contrary, M-Na-Clino particles seem to be less aggregate than B-Clino and M-Clino (Fig. 3e). At higher magnification, the scales of M-Clino are finer and more spaced than the ones of B-Clino, while M-Na-Clino flakes are more similar to the ones of B-Clino (Fig. 3b, d, and f). In light of this, the mesopores and macropores probably coincide with these distances. HR-TEM images of the supports reveal that the acid/alkaline attacks maintained the flaky morphology of clinoptilolite (Fig.4a) but modified the aspect of the flakes. The M-Clino (Fig. 4b) seems to

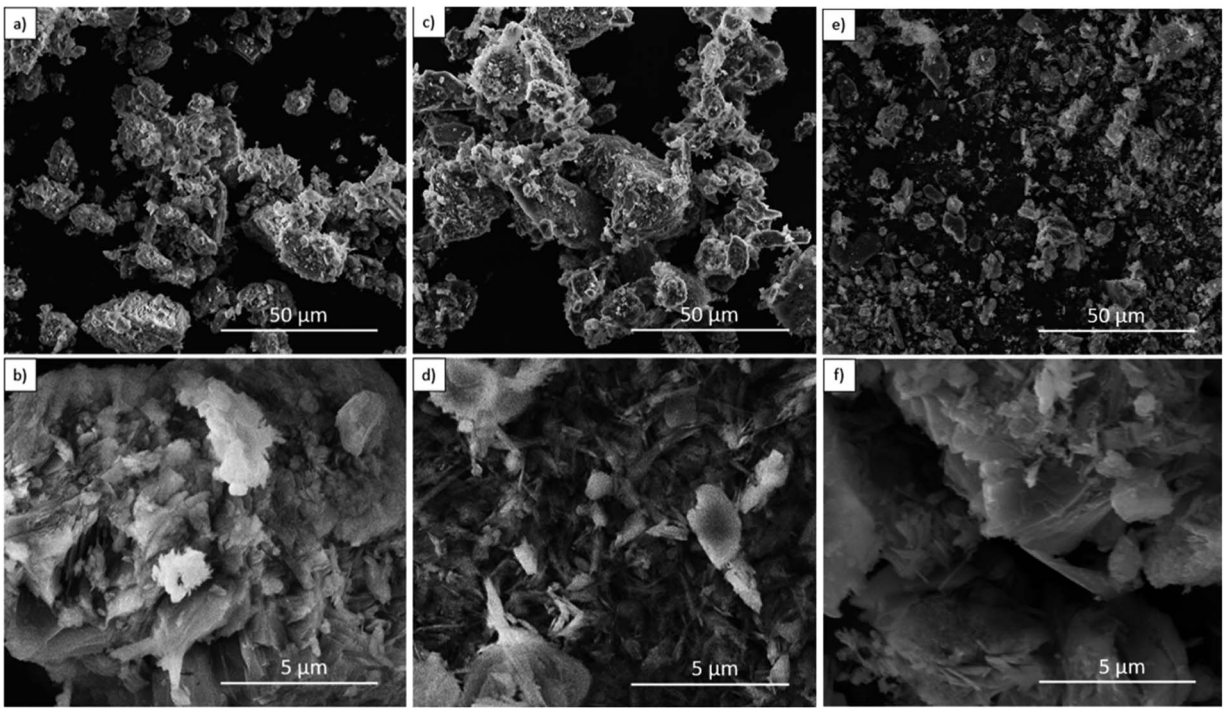

Fig. 3 FE-SEM images for B-Clino (a, b), M-Clino (c, d), and M-Na-Clino (e, f) at magnification 1k× and 10k×.

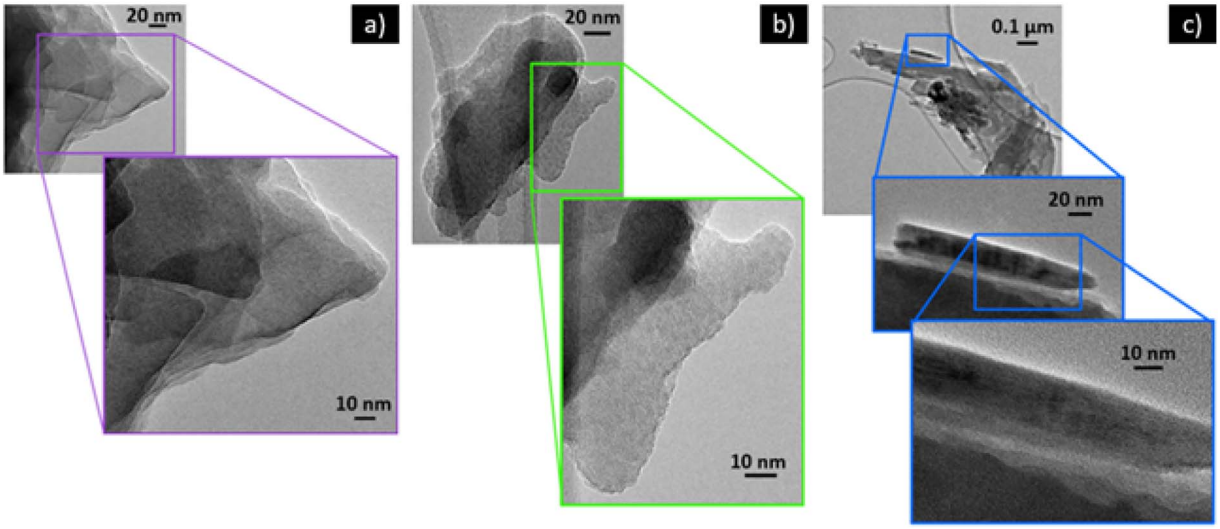

Fig. 4 HR-TEM images of (a) B-Clino (b) M-Clino and (c) M-Na-Clino samples.

have been eroded by acid/alkaline attacks; in fact, the edges look smoother, and the surface of the flakes appears rougher. These changes to flakes contributed to increase the surface area, as confirmed by the N_2 physisorption analysis. On the other hand, the M-Na-Clino (Fig. 4c) exhibits sharper edges than B-Clino and M-Clino. Moreover, it presents small particles partially incorporated into the structure (one of them is highlighted in the figure). These particles are different from the surrounding material and exhibit a more organized structure, it is possible to recognize parallel rows.

3.1.4 FT-IR spectroscopy. FT-IR measurements were conducted on the three different supports used for the immobilization of FDH and GlyDH. The IR spectra are reported in Fig. 5.

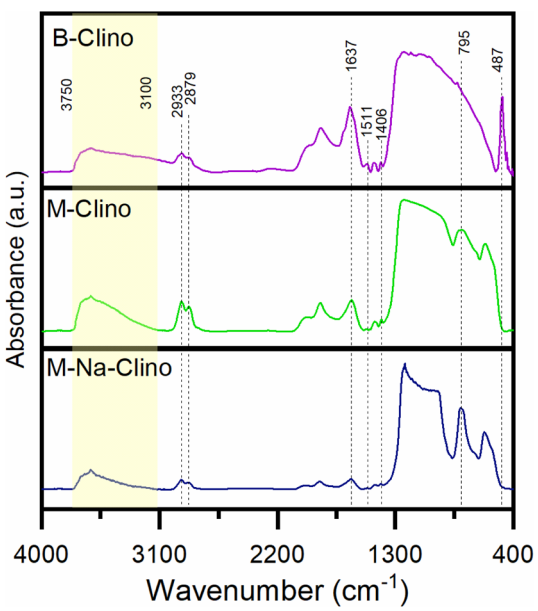

Fig. 5 FT-IR spectra in absorbance of the three functionalized supports: B-Clino, M-Clino, M-Na-Clino.

The spectra confirm the correct functionalization of the supports because all the samples present bands related to the vibration of ammino groups and to the organosilanes (CH_2) used for functionalizing the supports. Moreover, the supports exhibit also peaks that can be correlated to the structure of the zeolite. A summary of the vibration bands is reported in Table 2. All samples present a band in the range 3100–3750 cm^{-1}, this can correspond to the tensile vibrations of –NH, provided by the functionalization process, and –OH still present in the material despite the pre-treatment, due to the high specific surface area of the material. The spectrum of B-Clino presents an absorption band centered at 487 cm^{-1}, that can correspond to the vibrations of the bonding T–O (where T is Si or Al of the zeolitic structure). The absence of this peak, in the two modified supports, can be due to the acid and alkaline attacks that have slightly changed the structure of the clinoptilolite as has been highlighted by the XRD analysis.

In addition, it is possible assuming that the M-Clino is the sample for which the process of functionalization has been the most effective: it has the highest ratio between the propylamine vibrational peaks, provided by APTES and GPTMS, and the stretching vibration peak O–T–O. The FT-IR spectra of the support alone, the functionalized support, and the enzymes individually and co-immobilized, for all the materials used are reported in Fig. S2.†

3.2 Immobilization and co-immobilization of FDH and GlyDH

FDH and GlyDH were individually immobilized and co-immobilized, following a two-step protocol, as previously described, on the three different zeolites. The hetero-functional supports are used to rapidly immobilize enzymes through a multipoint covalent attachment. This technique can be used to immobilize different proteins.[25] The first step conducted at pH 7 enables the formation of ionic interactions between the enzymes and the amine groups provided by APTES; while the

Table 2 Absorption bands for B-Clino, M-Clino, and M-Na-Clino functionalized with APTES and GPTMS

Vibrational features	Wavenumber (cm^{-1})	Reference
Vibration T–O	487	34
Stretching O–T̂–O	795	34 and 35
Deformation Si–CH_2	1406	36
Bending C–N and bending N–H	1511	37
Water associated with Na and Ca in the zeolite channels	1637	37 and 38
Symmetric vibration CH_2	2879	36
Asymmetric vibration CH_2	2933	35 and 36
Tensile vibration –OH and –NH	3750–3100	26 and 35

second step at pH 10 promotes the creation of Schiff's bases between Lysine residues and the glyoxyl groups introduced in the support. The last step of the immobilization involves the use of sodium borohydride to reduce the Schiff's bases and finally obtain covalent bonds. This technique enables the use of hydrophobic support and high ionic strength solutions to be avoided. For example, with epoxy hydrophobic support 1 M buffer phosphate solutions are usually used.[25] The immobilization yields (IY) are 100% for all the immobilizations performed. The other immobilization metrics (retained activity, R_{act}; and specific activity, A_{IE}) of GlyDH and FDH separately immobilized and co-immobilized on the supports are reported in Table 3. Both enzymes immobilized on the mesostructured materials displayed an increased retained activity if compared to the ones on B-Clino. The retained activities obtained immobilizing FDH and GlyDH on the mesostructured zeolites are very similar: the R_{act} of GlyDH separately immobilized is better on M-Clino, R_{act} of FDH co-immobilized with GlyDH is slightly higher using M-Clino as support, on the contrary, the R_{act} of co-immobilized GlyDH is a bit lower on M-Clino. The retained activity obtained on the three supports is comparable with other works where the expressed activity ranged from 5% to 90% with FDH from *Candida boidinii* immobilized on glyoxyl agarose.[39] In our previous works, FDH on glyoxyl silica showed a retained activity of 10–14%, while with FDH on glyoxyl or amino natural zeolite a retained activity from 4 to 40% was obtained.[15,16] Approximating the shape of the two enzymes with a sphere,[40] a diameter of 5.54 nm and 8.99 nm is obtained, starting with molecular weights of 74 kDa,[41] and 31.6 kDa,[42] respectively for FDH and GlyDH. Moreover, GlyDH is a multimeric enzyme composed of 8 subunits,[42] therefore the loss of activity during immobilization is likely due to the dissociation of its units and their desorption from the support.[43] M-Clino support allows to obtain the best R_{act} of co-immobilized FDH, and although the R_{act} of co-immobilized GlyDH is slightly lower, it is still sufficiently high to perform the reaction. The yields of immobilization and retained activities of GlyDH are comparable with those obtained by Rocha-Martin and colleagues on glyoxyl agarose,[29] with immobilization yields in the 70–100% range and expressed activities in the 5–40% range. The specific activity of the co-immobilized FDH resulted to be approximately 2.5 times the one of GlyDH presents on the same support. For this reason, a further co-immobilization with the ratio of 1 : 4 by weight between FDH and GlyDH was performed, to increase the specific activity of the biocatalyst. Also, the IY of this last co-immobilization resulted to be 100%. The specific activity (A_{IE}) calculated for the co-immobilized FDH (1 : 4 ratio by weight) is 2.34 UI g^{-1} while the one of GlyDH is 1.35 UI g^{-1}. Using a 1 : 4 loading ratio of the two enzymes, the specific activity gap is reduced, in this case, the A_{IE} of FDH resulted to be approximately 1.7 times the one of GlyDH.

3.3 Characterization of biocatalysts

3.3.1 Distribution of the enzymes. To understand the influence of the structural changes on the zeolite, a study of the distribution of the enzymes was carried out. For that purpose, the enzymes were labeled with fluorescence dyes, FDH and GlyDH with ATTO 488 dye and ATTO 550, respectively. The images collected with the fluorescence microscope depict a grain of the clinoptilolite in brightfield (Fig. 6a).

FDH is reported in the green emission channel (Fig. 6c), and GlyDH, thus is expected to visualize in the red emission channel (Fig. 6d). Besides, unloaded B-Clino was observed with the same parameters to check that the support itself has no fluorescence emission, as reported in the ESI (Fig. S3†). On the contrary, mesostructured supports (M-Clino and M-Na-Clino) themselves have fluorescence emission preventing the observation of the enzyme, probably due to the reagent used for the mesostructuring and functionalization process. For this reason, the images of FDH and GlyDH immobilized on M-Clino and M-Na-Clino are not reported. From the merged image (Fig. 6b), the two enzymes appear not to be equally distributed over the zeolite particle. In particular, the signal related to ATTO 488 (green), corresponding to FDH, seems to be more uniformly spread, while the one by ATTO 550 (red), labeled GlyDH, is more likely confined on the edges. This can be attributed to the different sizes of the two enzymes, which causes GlyDH to remain at the edges of the particle. This heterogeneous distribution opens opportunities for the development of positional

Table 3 Retained activity (R_{act}) and specific activity (A_{IE}) of biocatalysts

	FDH		FDH co-imm.		GlyDH		GlyDH co-imm.	
	A_{IE} (IU g^{-1})	R_{act} (%)	A_{IE} (IU g^{-1})	R_{act} (%)	A_{IE} (IU g^{-1})	R_{act} (%)	A_{IE} (IU g^{-1})	R_{act} (%)
B-Clino	0.64	18	0.05	3	0.29	16	0.09	9
M-Na-Clino	3.22	89	1.45	80	0.40	22	0.77	83
M-Clino	3.17	88	1.68	93	0.65	35	0.69	74

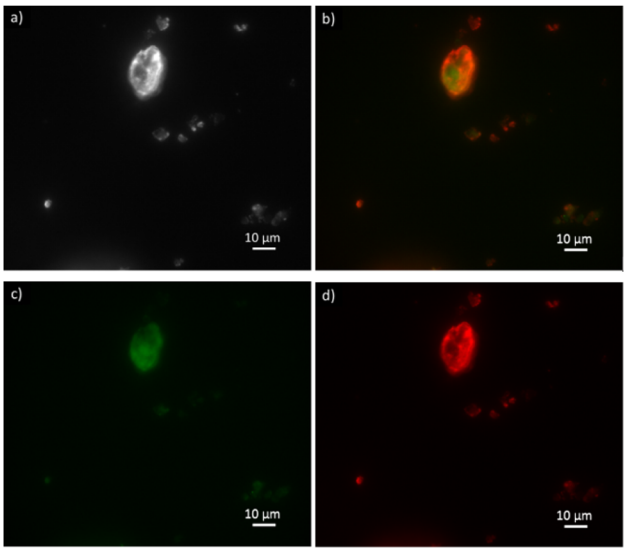

Fig. 6 Optical fluorescence microscopy images of clinoptilolite (a) with ATTO-488 labeled FDH enzyme in the green channel (c) and ATTO-550 labeled GlyDH enzyme in the red channel (d) co-immobilized over B-Clino. Image (b) shows the two enzymes in the red and green channels. The image (a) is in brightfield.

co-immobilization on zeolites.[44,45] Furthermore, it raises the question of how the distribution of the enzymes is in the mesostructured zeolites, but unfortunately as mentioned before the autofluorescence of the material did not allow to observe the enzyme distribution. In any case, the fluorescence microscopy also shows the co-presence of the two enzymes in the same sites of the support particles: this is a confirmation of having effectively co-immobilized FDH and GlyDH on Clinoptilolite particles.

3.3.2 Effect of temperature and pH on biocatalysts activity. To determine the optimal pH and temperature of the two enzymes in different operational conditions, the enzymatic activity was measured by changing the pH or temperature concerning the conditions described in Section 2.2.5. For the sake of brevity, the tests were performed to have a comparison between the free enzymes, the enzymes separately immobilized (FDH/MClino or GlyDH/MClino), and co-immobilized (FDHco-imm/MClino or GlyDH co-imm/MClino) on mesostructured clinoptilolite (M-Clino), the material used as support. The results for the optimal temperature are reported in Fig. 7, while the corresponding values of optimal pH are in Fig. 8. Both free FDH and GlyDH showed their maximum activity at 50 °C. FDH immobilized over M-Clino was most active at 60 °C, with a shift of 10 °C in optimal temperature. Regarding the GlyDH enzyme on M-Clino, the trend is very similar to that of the free enzyme. Being supported over M-Clino seems slightly unfavorable for both enzymes and the two curves appear to be narrower. Also in our previous works, with FDH on glyoxyl or amino mordenite and glyoxyl silica, an increase in optimal temperature was not obtained.[15,16] Concerning the behavior of co-immobilized enzymes, the co-presence of FDH and GlyDH on the same support seems to increase the activity at a lower temperature, FDH is most active at 60 °C while GlyDH is at 50 °C, and the optimal temperature is the same obtained for the enzymes separately immobilized. As far as pH is concerned, the two free enzymes are characterized by significantly different optimal values, around 7 for FDH and up to 10 for GlyDH. This becomes a problem in the context of a chain reaction that involves both. On the other hand, the optimal pH of GlyDH supported over M-Clino is shifted towards 8, closing the gap with FDH pH. On the contrary, GlyDH co-immobilized with FDH over M-Clino is qualified by an optimal pH of around 9. Nevertheless, co-immobilized FDH presents generally higher stability than the

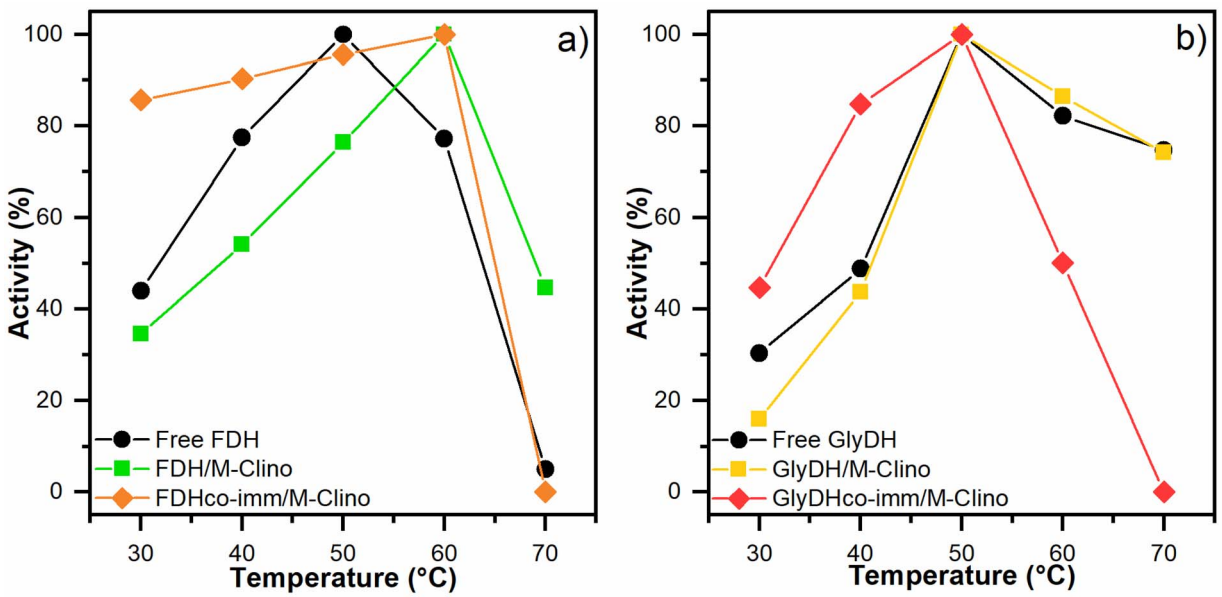

Fig. 7 Optimal temperature results for FDH (a) and GlyDH (b). The tests were performed several times.

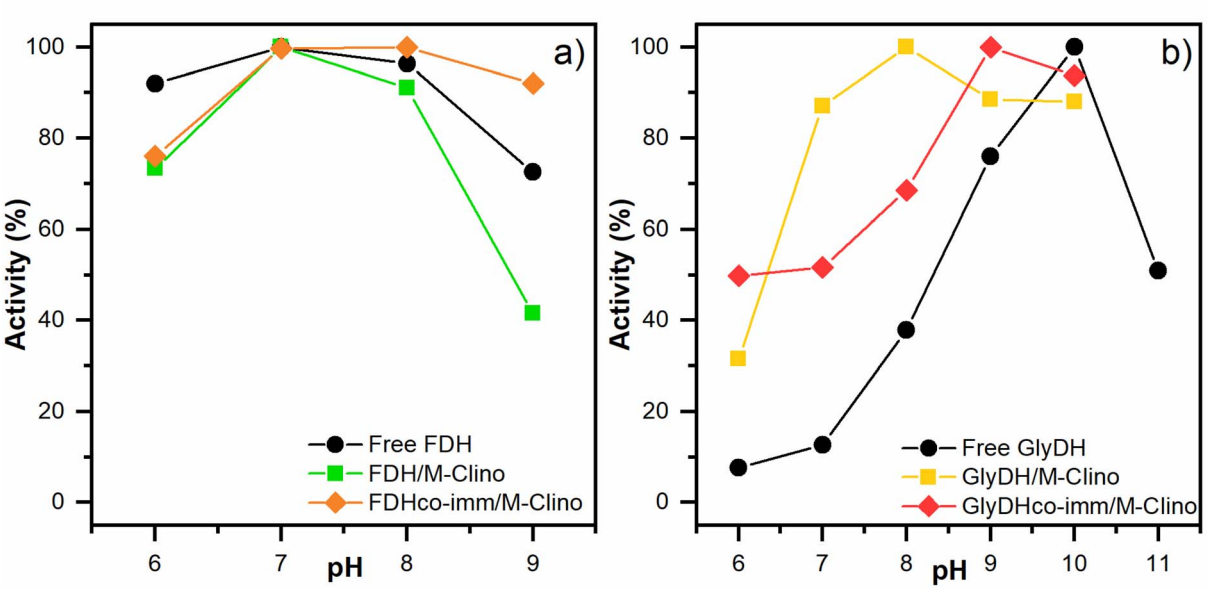

Fig. 8 Optimal pH results for FDH (a) and GlyDH (b). The tests were performed many times.

free or individually immobilized enzyme, which is most active at pH 8. So, the gap between FDH and GlyDH remains constant.

3.3.3 Thermal stability of free and immobilized enzymes. The kinetic of thermal deactivation was represented as the percentage of the initial activity, the results are shown in Fig. 9. The tests were carried out only on the biocatalysts obtained immobilizing the enzymes on M-Clino. Free FDH displayed exponential deactivation kinetics, described by eqn (4). While the loss of activity of immobilized enzymes and free GlyDH was described using eqn (5) since at the end of the test a residual activity was observed. Table 4 summarizes the main parameters for the models used to describe the thermal deactivation of the different biocatalysts, namely deactivation constant K_D, residual activity R_{act}, and half-life $t_{1/2}$. The stability of FDH was visibly enhanced by the immobilization over mesostructured zeolite, obtaining an increase in terms of half-life. Furthermore, the biocatalyst had a residual activity of 40%, while the residual activity of the free enzyme was under 10% after 72 hours. The stabilization factor of FDH/M-Clino (around 2.7) is comparable to the results present in the literature. For example, with *Candida methylica* FDH immobilized on aldehyde immobead 150, a stabilization factor of 3.6 was obtained.[46] In our previous

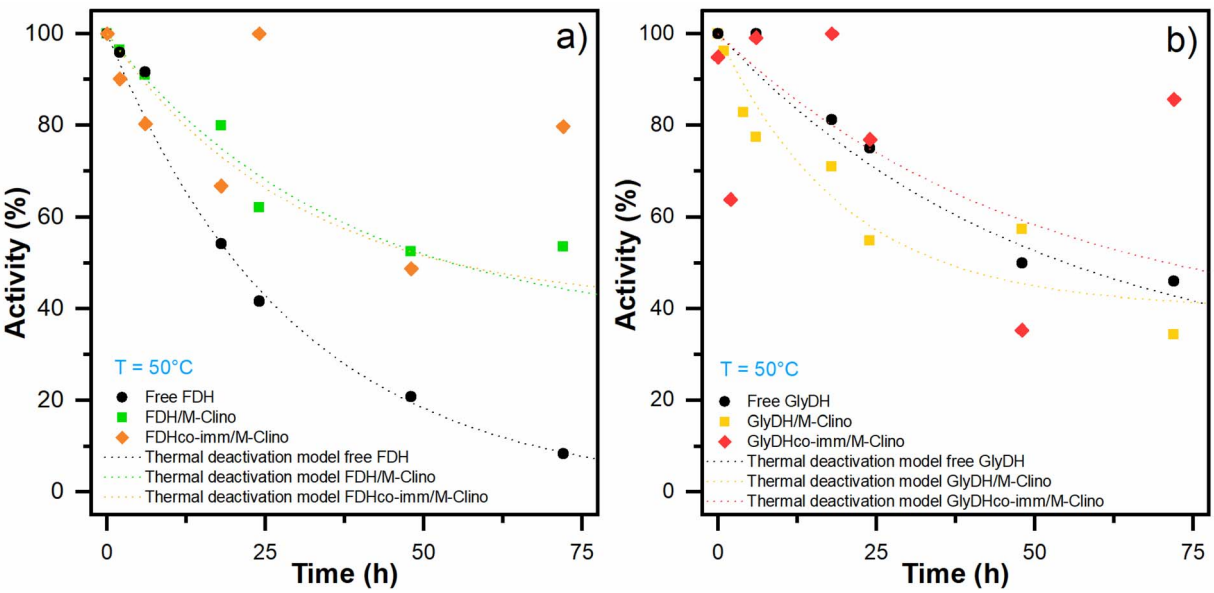

Fig. 9 Thermal deactivation of FDH (a) and GlyDH (b): thermal deactivation models for the soluble enzyme (black dot line) and the enzyme immobilized on M-Clino separately (FDH green dot line, GlyDH yellow dot line), and co-immobilized (FDH orange dot line, GlyDH red dot line). The points had been replicated.

Table 4 Thermal deactivation kinetic parameters for FDH and GlyDH derivates at 50 °C

	Free FDH	FDH/M-Clino	FDH co-imm/M-Clino	Free GlyDH	GlyDH/M-Clino	GlyDH co-imm/M-Clino
Decay constant K_D (h^{-1})	0.034	0.027	0.037	0.020	0.050	0.020
Residual activity α	0	0.35	0.40	0.25	0.40	0.34
Half-life time $t_{1/2}$ (h)	20	54	48	55	36	71

works, an F_S of 3.7 and 18.9 was obtained, respectively with *Candida boidinii* FDH immobilized respectively on glyoxyl $MCF_{0.75}$ and amino mordenite.[15,16]

With glyoxyl agarose, a stabilization factor of 150 by Bolivar and colleagues was obtained.[39] To enhance the biocatalyst stability, the immobilization rate could be optimized, as observed by Mateo and co-workers.[47] When FDH is co-immobilized with GlyDH similar results are obtained.

Regarding the stability of GlyDH, no significant differences were observed between its immobilized and soluble forms.

The structural complexity of GlyDH, its large size, and the composition of 8 subunits, make its stabilization very complex. Increased stability of this enzyme has only been reported when its quaternary structure has been stabilized by crosslinking with polymers.[29] Considering that both enzymes have similar lifetimes, the use of this type of modification with polymers was discarded.

3.4 CO_2 reduction

To carry out the CO_2 reduction a 0.1 M buffer phosphate pH 7 was used to avoid the deactivation of the cofactor, which happens at a more basic or acidic pH, during the reaction.[48] Furthermore, even if the highest activity was observed at 50 °C, the reaction was carried out at room temperature and atmospheric pressure. Higher temperatures have the drawback of substantially reducing the CO_2 solubility in aqueous media and it causes a faster deactivation of cofactor.[48,49] The results of the reactions were evaluated by monitoring the production of formic acid (the concentration of DHA in the solution was not measured).

Samples of the reacting mixture were collected periodically to evaluate formic acid concentration, for the different reactions. The first reaction is carried out only with FDH supported over M-Clino using NADH 10 mM as a reducing agent, and the results are shown in Fig. S4a.† The second reaction is carried out using FDH and GlyDH co-immobilized on M-Clino (a scheme of the two reactions catalyzed by FDH and GlyDH is reported in Fig. 10a), in this case starting with NAD^+ 10 mM, this reaction is conducted in two different cases varying the FDH : GlyDH w/w weight ratio during the immobilization procedure (FDH : GlyDH 1 : 1 ratio and FDH : GlyDH 1 : 4 ratio in Fig. S4b and c† respectively). In these tests, the oxidized form of the nicotinamide cofactor was added (NAD^+), with glycerol in the solution. If formic acid is observed, the regeneration of the reduced form of the cofactor (NADH) carried out by the GlyDH enzyme is confirmed. Fig. 10b shows the maximum concentration of formic acid obtained in the solution for the three reaction conditions.

The reduction of CO_2, performed by FDH over M-Clino, proceeds successfully (Fig. S4a†), providing a peak of 5.5 mM of formic acid after 2 hours of reaction. This means that the mass production of formic acid, related to the activity of FDH, is 2.65 mg IU_{FDH}^{-1}. At equilibrium, the conversion settles down at around 50%. A similar result was obtained in our previous work, where a concentration of about 4 mM of formic acid was observed with FDH on glyoxyl and amino mordenite.[16]

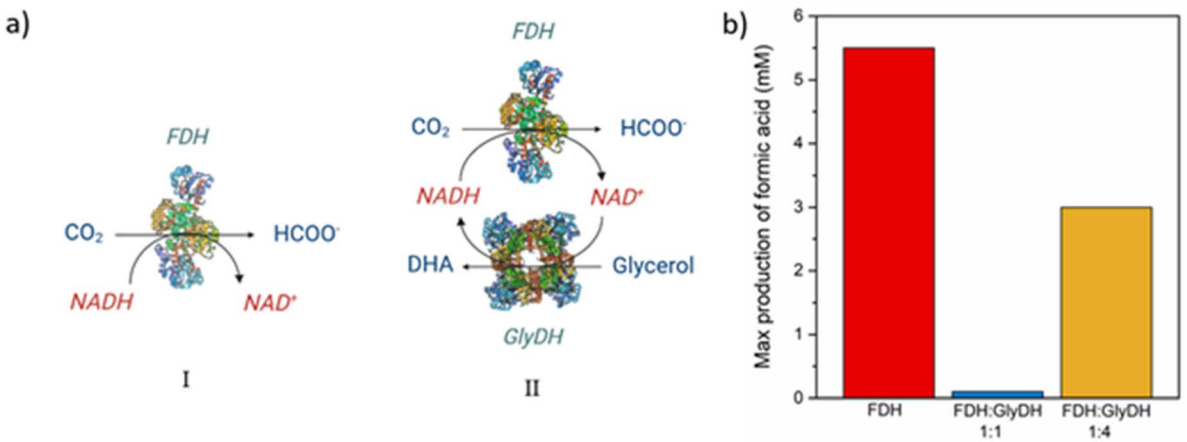

Fig. 10 (a) Scheme of the reactions of CO_2 conversion into formic acid in the presence of NADH catalyzed by FDH(i) CO_2 conversion and oxidation of NAD^+ to obtain and regenerate NADH, catalyzed respectively by FDH and GlyDH co-immobilized on M-Clinoptilolite(ii). (b) Maximum concentration of formic produced after 2 hours of reaction due to the reduction of CO_2 by FDH (red) FDH : GlyDH w/w ratio 1 : 1 (blue) FDH : GlyDH w/w ratio 1 : 4 (yellow).

The reaction catalyzed by FDH, with cofactor regenerated by GlyDH, with the same amount in weight of the two enzymes, instead, produced around 100 μM of formic acid (Fig. S4b†). This indicates a mass production of formic acid, related to the activity of FDH, of about 0.05 mg IU_{FDH}^{-1}. These performances may be due to the first reaction of the chain, catalyzed by GlyDH, which is slower than the reaction catalyzed by FDH, producing a "bottleneck" phenomenon. In this case, the formic acid produced is very little, so the concentration of NADH regenerated by GlyDH is not enough to permit a reduction of CO_2 catalyzed by FDH. In light of this, to improve the reaction, the loading ratio (in weight) of FDH/GlyDH was raised to 1 : 4.

By increasing the amount of GlyDH, NADH was produced in a greater amount by oxidizing glycerol to 1,3-dihydroxyacetone, improving the reaction condition, compared to the previous case. Therefore, the regenerated NADH is used to reduce CO_2 to formic acid. It is possible to see the reaction mechanism in Fig. 10a-II. After 2 h a maximum of 3 mM of formic acid is reached. This implies that the mass production of formic acid, related to the activity of FDH, is 1.44 mg IU_{FDH}^{-1}. In this way, it is also possible to confirm the regeneration of the NADH cofactor. Subsequently, a part of formic acid is converted back to CO_2, in fact after 4 hours the concentration of formic acid in the solution is about 1.5 mM (Fig. S4c†). As the reaction goes ahead, GlyDH is progressively subjected to product inhibition, because DHA is not removed from the reacting medium.[50] As a result, the rate of NADH regeneration becomes slower until it reaches zero. This decrease in the regeneration rate leads to an accumulation of NAD^+ in the media, which shifts the direction of the reaction to the consumption of formic acid. Finally, after 6 hours a concentration of 2 mM of formic acid was observed, but it does not achieve the maximum reached after 2 hours.

Rocha-Martin and colleagues reported that the GlyDH, as a free enzyme, has a half-maximal inhibitory concentration (IC_{50}) of DHA, produced by the oxidation of glycerol, equal to 0.43 mM.[29] Furthermore, its acid sites are the most commonly used to carry out the immobilization on hetero-functionalized support. These sites mainly correspond to the active sites where the non-competitive inhibition by DHA takes place, as demonstrated by Rocha-Martin *et al.* using a 3D structure,[29] increasing the half-maximal inhibitory concentration. To avoid this inhibition and recover the DHA product, alternatives such as *in situ* product removal have been proposed.[51] This could be a strategy to enhance the regeneration of the cofactor and facilitate the purification of the products of the reaction.

The immobilization of FDH and GlyDH on hetero-functionalized support, even if it does not allow an increase in thermal stability, it could be used to carry out CO_2 reduction with a biocatalyst that can be recovered and potentially re-used.

4 Conclusions

The conversion of CO_2 to formic acid was evaluated using the enzyme FDH from *Candida boidinii*, covalently immobilized on the hetero-functionalized clinoptilolite. For the first time, the FDH enzyme was co-immobilized on porous support along with the GlyDH enzyme from *Geobacillus stearothermophilus*, capable of carrying out a regeneration of the NADH cofactor.

In particular, the influence of the surface area and the support morphology was investigated. A mesostructuring process was carried out on the support using an acid/base treatment. Through physisorption with N_2 at −196 °C, a noticeable increase in surface area and an enlargement of the pores were observed. To carry out a covalent immobilization, a process of hetero-functionalization using APTES and GPTMS was performed. In this way, amino and glyoxyl groups were generated on the supports and the immobilization was carried out on both the pristine support and the mesostructured ones. The co-immobilization and co-localization of both enzymes were confirmed by fluorescence microscopy.

An increase in the activity of the two enzymes was observed when they are immobilized on mesostructured clinoptilolite compared to when untreated clinoptilolite is used as support. Both the free and immobilized enzymes were characterized for optimal pH and T. In addition, a thermal stability test at 50 °C was performed, demonstrating a significant increase in half-life for the FDH enzyme. The GlyDH enzyme, on the other hand, is more stable in free than immobilized form.

Finally, the two enzymes were used to carry out the reduction of CO_2 to formic acid. FDH alone produced a concentration of 5 mM, resulting in a conversion of approximately 50% compared to the initially provided NADH cofactor. The reduction reaction was also possible using the two co-immobilized enzymes and starting from the cofactor in an oxidized form. The GlyDH enzyme, using glycerol, generated NADH starting from NAD^+ which was then used by the FDH enzyme to carry out the reduction reaction. In this case, at the end of the test, a concentration of about 2 mM of formic acid was obtained. On the other hand, to increase the performance, it would be possible to extract the two enzymes from different microorganisms that are more efficient in carrying out these two reactions.

The strategy of mesostructuring the porous materials and the subsequent immobilization seems very promising and paves the way for the future development of processes applied to a wider array of enzymes.

Author contributions

Conceptualization: M. P., C. O.; methodology: M. P., C. O., T. T.; investigation: G. P., C. C., I. Z., M. D., O. R., V. C.; funding acquisition: C. O., O. R.; resources: M. P., C. O., T. T., V. C., D. F., writing – original draft: I. Z., G. P., C. C.; writing – review and editing: O. R., T. T. C. C.; supervision: M. P., C. O.

Conflicts of interest

There are no conflicts to declare.

Acknowledgements

Politecnico di Torino for the funding support required to publish this work in gold open access. O. R. acknowledges the

support of Generalitat de Catalunya AGAUR for a Beatriu de Pinós H2020 MSCA-Cofund (2019-BP-00180). The funding support provided by ANID-Chile through the project FONDECYT 11180967 is acknowledged.

Notes and references

1 S. K. Bhatia, R. K. Bhatia, J. M. Jeon, G. Kumar and Y. H. Yang, *Renewable Sustainable Energy Rev.*, 2019, **110**, 143–158.

2 P. R. Yaashikaa, P. Senthil Kumar, S. J. Varjani and A. Saravanan, *J. CO2 Util.*, 2019, **33**, 131–147.

3 M. Aresta and A. Dibenedetto, *Dalton Trans.*, 2007, **28**, 2975–2992.

4 A. M. Appel, J. E. Bercaw, A. B. Bocarsly, H. Dobbek, D. L. Dubois, M. Dupuis, J. G. Ferry, E. Fujita, R. Hille, P. J. A. Kenis, C. A. Kerfeld, R. H. Morris, C. H. F. Peden, A. R. Portis, S. W. Ragsdale, T. B. Rauchfuss, J. N. H. Reek, L. C. Seefeldt, R. K. Thauer and G. L. Waldrop, *Chem. Rev.*, 2013, **113**, 6621–6658.

5 J. Shi, Y. Jiang, Z. Jiang, X. Wang, X. Wang, S. Zhang, P. Han and C. Yang, *Chem. Soc. Rev.*, 2015, **44**, 5981–6000.

6 R. Obert and B. C. Dave, *Ind. Eng. Chem. Res.*, 1998, **37**, 12192–12193.

7 S. Kuwabata, R. Tsuda and H. Yoneyama, *Electrochemical Conversion of Carbon Dioxide to Methanol with the Assistance of Formate Dehydrogenase and Methanol Dehydrogenase as Biocatalysts*, 1994, vol. 116.

8 C. Mateo, J. M. Bolivar, C. A. Godoy, J. Rocha-Martin, B. C. Pessela, J. A. Curiel, R. Muñoz, J. M. Guisan and G. Fernández-Lorente, *Biomacromolecules*, 2010, **11**, 3112–3117.

9 S. Velasco-Lozano, A. I. Benítez-Mateos and F. López-Gallego, *Angew. Chem.*, 2017, **129**, 789–793.

10 F. Marpani, M. Pinelo and A. S. Meyer, *Biochem. Eng. J.*, 2017, **127**, 217–228.

11 A. Dibenedetto, P. Stufano, W. Macyk, T. Baran, C. Fragale, M. Costa and M. Aresta, *ChemSusChem*, 2012, **5**, 373–378.

12 H. Song, C. Ma, P. Liu, C. You, J. Lin and Z. Zhu, *J. CO_2 Util.*, 2019, **34**, 568–575.

13 R. Cazelles, J. Drone, F. Fajula, O. Ersen, S. Moldovan and A. Galarneau, *New J. Chem.*, 2013, **37**, 3721–3730.

14 I. Poljungreed and S. Boonyarattanakalin, *J. Chem. Technol. Biotechnol.*, 2017, **92**, 2635–2641.

15 G. Pietricola, T. Tommasi, M. Dosa, E. Camelin, E. Berruto, C. Ottone, D. Fino, V. Cauda and M. Piumetti, *Int. J. Biol. Macromol.*, 2021, **177**, 261–270.

16 G. Pietricola, C. Ottone, D. Fino and T. Tommasi, *J. CO_2 Util.*, 2020, **42**, 101343.

17 E. Camelin, O. Romero, M. Piumetti, C. Ottone, A. Illanes and D. Fino, in *Nanomaterials for biocatalysis*, Elsevier, 2021, pp. 105–148.

18 M. Sprynskyy, B. Buszewski, A. P. Terzyk and J. Namieśnik, *J. Colloid Interface Sci.*, 2006, **304**, 21–28.

19 C. Galletti, M. Dosa, N. Russo and D. Fino, *Environ. Sci. Pollut. Res.*, 2021, **28**, 24355–24361.

20 S. Mitchell and J. Pérez-Ramírez, *Catal. Today*, 2011, **168**, 28–37.

21 M. Hartmann and D. Jung, *J. Mater. Chem.*, 2010, **20**, 844–857.

22 N. Ramírez, M. Serey, A. Illanes, M. Piumetti and C. Ottone, *J. Photochem. Photobiol., B*, 2021, **215**, 112113.

23 A. Illanes, *Enzyme biocatalysis: Principles and applications*, Springer, 2008.

24 R. C. Rodrigues, Á. Berenguer-Murcia, D. Carballares, R. Morellon-Sterling and R. Fernandez-Lafuente, *Biotechnol. Adv.*, 2021, **52**, 107821.

25 *Immobilization of Enzymes and Cells*, ed. J. M. Guisan., Humana Totowa, NJ, 3rd edn, 2013.

26 D. Verboekend, T. C. Keller, M. Milina, R. Hauert and J. Pérez-Ramírez, *Chem. Mater.*, 2013, **25**, 1947–1959.

27 S. Arana-Peña, D. Carballares, R. Morellon-Sterlling, Á. Berenguer-Murcia, A. R. Alcántara, R. C. Rodrigues and R. Fernandez-Lafuente, *Biotechnol. Adv.*, 2021, **51**, 107584.

28 M. M. Bradford, *Anal. Biochem.*, 1976, **72**, 248–254.

29 J. Rocha-Martin, A. Acosta, J. Berenguer, J. M. Guisan and F. Lopez-Gallego, *Bioresour. Technol.*, 2014, **170**, 445–453.

30 M. Moradi, R. Karimzadeh and E. S. Moosavi, *Fuel*, 2018, **217**, 467–477.

31 C. Bernal, L. Sierra and M. Mesa, *J. Mol. Catal. B: Enzym.*, 2012, **84**, 166–172.

32 J. M. Guisán, *Enzyme Microb. Technol.*, 1988, **10**, 375–382.

33 J. Rocha-Martín, B. de Las Rivas, R. Muñoz, J. M. Guisán and F. López-Gallego, *ChemCatChem*, 2012, **4**, 1279–1288.

34 H. Faghihian and M. Kabiri-Tadi, *J. Hazard. Mater.*, 2010, **178**, 66–73.

35 M. Babazadeh, H. Abolghasemi, M. Esmaeili and A. Ehsani, *Sep. Purif. Technol.*, 2021, **267**, 118601.

36 N. Majoul, S. Aouida and B. Bessaïs, *Appl. Surf. Sci.*, 2015, **331**, 388–391.

37 S. Nezamdoust and D. Seifzadeh, *Prog. Org. Coat.*, 2017, **109**, 97–109.

38 J. Kabuba and M. Banza, *Results Eng.*, 2020, **8**, 100189.

39 J. M. Bolivar, L. Wilson, S. A. Ferrarotti, R. Fernandez-Lafuente, J. M. Guisan and C. Mateo, *Enzyme Microb. Technol.*, 2007, **40**, 540–546.

40 H. P. Erickson, *Biol. Proced. Online*, 2009, **11**, 32–51.

41 H. Schutte, J. Flossdorf, H. Sahm and M.-R. Kula, *Eur. J. Biochem.*, 1976, **62**, 151–160.

42 S. N. Ruzheinikov, J. Burke, S. Sedelnikova, P. J. Baker, R. Taylor, P. A. Bullough, N. M. Muir, M. G. Gore and D. W. Rice, *Structure*, 2001, **9**, 789–802.

43 R. Fernandez-Lafuente, *Enzyme Microb. Technol.*, 2009, **45**, 405–418.

44 S. Velasco-Lozano and F. López-Gallego, *Biocatal. Biotransform.*, 2018, **36**, 184–194.

45 A. H. Orrego, F. López-Gallego, G. Fernandez-Lorente, J. M. Guisan and J. Rocha-Martín, *Methods Mol. Biol.*, 2020, **2100**, 297–308.

46 B. Binay, D. Alagöz, D. Yildirim, A. Çelik and S. Seyhan Tükel, *Beilstein J. Org. Chem.*, 2016, **12**, 271–277.

47 C. Mateo, O. Abian, R. Fernandez-Lafuente and J. M. Guisan, *Enzyme Microb. Technol.*, 2000, **26**, 509–515.

48 O. H. Lowry, J. V. Passonneau and M. K. Rock, *J. Biol. Chem.*, 1961, **236**, 2756–2759.
49 R. H. Perry and D. W. Green, *Perry's Chemical Engineers' Handbook*, 8th edn, McGraw-Hill, 2007.
50 M. Piumetti, *Molecular Dynamics and Complexity in Catalysis and Biocatalysis*, Nature, First., 2022.
51 Y. Q. Peng, S. Z. Wang, L. Lan, W. Chen and B. S. Fang, *Eng. Life Sci.*, 2013, **13**, 479–486.